Ellipsoidal models for four-image lenses: implications for galactic structure and H_0

C. R. Keeton & C. S. Kochanek

Harvard-Smithsonian Center for Astrophysics, MS-51
60 Garden Street, Cambridge, MA 02138

Abstract. Several 4-image lenses cannot be fit by simple ellipsoidal mass distributions, but can be fit by adding an additional shear. In lenses such as PG 1115+080 and B 1422+231 (as well as the radio ring MG 0751+2716) the shear arises from small groups containing the lens galaxies, but in other lenses the shear may be internal to the lens galaxy and could offer insight into properties like triaxiality. The additional shear introduces degeneracies into lens models, and attempts to use lenses to determine the Hubble constant must examine the degeneracies to understand systematic effects in H_0. We illustrate these effects with new models of B 1608+656 showing the need for an additional shear whose source is difficult to explain.

1. Introduction

Gravitational lensing provides a new and exciting way to study astrophysics and cosmology. Image configurations directly probe the mass distributions of distant galaxies, time delays give a distance scale and hence determine the Hubble constant H_0, and lens statistics probe cosmological parameters such as λ_0. The first two applications require good knowledge of the lensing potential, which means both finding a model for the potential that can reproduce the observations in quantitative detail, and exploring the parameters space to understand the systematic uncertainties in the model.

A good way to study lensing potentials is to apply ellipsoidal lens models to 4-image lenses. Lens models based on an ellipsoidal mass distribution probe a physically plausible quadrupole structure. The important isothermal ellipsoid model has an analytic form that is almost as easy to use as the popular singular isothermal sphere plus external shear model (see §2). Four-image lenses offer more data than two-image lenses and thus better constrain lens models. In addition, although 4-image lenses have fewer constraints than radio rings, they are significantly easier to model and thus allow large surveys of parameter space to understand degeneracies and systematic effects.

This talk will discuss some implications from models of 4-image lenses on galactic structure and H_0. §2 presents the formulation for ellipsoidal lens models and gives analytic results for the isothermal ellipsoid. §3 discusses general features of models of 4-image lenses. §4 illustrates some of these features with new models of B 1608+656. §5 summarizes the conclusions.

2. Ellipsoidal Lens Models

The projection of an ellipsoidal mass distribution is an elliptical surface mass density, which we write in the form

$$\Sigma = \Sigma(m^2), \qquad \text{where} \qquad m^2 = r^2[1 + \varepsilon \cos 2(\theta - \theta_0)], \tag{1}$$

where ε is a natural ellipticity parameter related to the projected axis ratio q by $q^2 = (1-\varepsilon)/(1+\varepsilon)$, and θ_0 is the orientation angle of the major axis defined as a standard position angle measured North through East. The projected axis ratio combines the intrinsic axis ratio and the inclination; for example, an oblate spheroid with intrinsic axis ratio q_3 and inclination i (where $i = 90°$ is face-on) has a projected axis ratio $q = (q_3^2 \cos^2 i + \sin^2 i)^{1/2}$. Only the projected axis ratio can be constrained by lensing.

The lensing properties of Σ are described by the lensing potential ϕ determined from the two-dimensional Poisson equation $\nabla^2 \phi = 2\Sigma/\Sigma_{cr}$, where Σ_{cr} is the critical surface density for lensing. Derivatives of the potential give the deflection angle and the magnification tensor (see Schneider, Ehlers & Falco 1992), and the potential itself enters the light travel time

$$\tau(\vec{x}) = \frac{1+z_l}{c} \frac{D_l D_s}{D_{ls}} \left(\frac{1}{2} |\vec{x} - \vec{u}|^2 - \phi(\vec{x}) \right), \tag{2}$$

where D_l, D_s, and D_{ls} are angular diameter distances to the lens, to the source, and from the lens to the source, respectively. The time delay between an image at $\vec{x}_i$ and an image at $\vec{x}_j$ is $\Delta\tau_{ij} = \tau(\vec{x}_i) - \tau(\vec{x}_j)$. The factor $D_l D_s / D_{ls}$ is inversely proportional to H_0, so with a measurement of $\Delta\tau_{ij}$ and a lens potential ϕ, we can use eq. (2) to determine H_0.

A versatile class of models consists of softened power-law ellipsoids with surface mass density

$$2\Sigma/\Sigma_{cr} = b^{2-\alpha} \left[s^2 + m^2 \right]^{\alpha/2 - 1}, \tag{3}$$

where α is the power law exponent such that $M(r) \propto r^\alpha$ asymptotically, s is a core radius, and b is the deflection scale. For $\alpha = 1$ this is a softened isothermal model, which is thought to represent dark matter distributions. For $\alpha = 0$ it is a modified Hubble model, which can be used to approximate constant mass-to-light ratio models. Also useful is the more centrally-concentrated $\alpha = -1$ model.

Analytic expressions for the lensing properties can be found for models with integer α. Of greatest interest is the softened isothermal model ($\alpha = 1$), for which the lensing potential, deflection, and magnification are

$$\phi = x\,\alpha_{,x} + y\,\alpha_{,y} - \frac{b\,s}{\sqrt{1-\varepsilon^2}} \ln \left[\frac{(\psi + s/q)^2 + 2\varepsilon x^2}{1+\varepsilon} \right]^{1/2} + \text{constant}, \tag{4}$$

$$\alpha_{,x} = \frac{b}{\sqrt{2\varepsilon}} \tan^{-1} \left[\frac{\sqrt{2\varepsilon}\, x}{\psi + s/q} \right], \tag{5}$$

$$\alpha_{,y} = \frac{b}{\sqrt{2\varepsilon}} \tanh^{-1} \left[\frac{\sqrt{2\varepsilon}\, y}{\psi + s\, q} \right], \tag{6}$$

$$M^{-1} \quad = \quad 1 - \frac{b}{\psi} - \frac{b^2 s}{q\,\psi\,[(\psi + s/q)^2 + 2\varepsilon x^2]}\ , \tag{7}$$

where $\psi^2 = s^2 + (1-\varepsilon)x^2 + (1+\varepsilon)y^2$. These results are taken from Keeton & Kochanek (1997b) but expressed in a slightly different form. They are equivalent to results derived by Kassiola & Kovner (1993) and Kormann, Schneider & Bartelmann (1994) but are written in a simpler form.

It is obvious that ellipsoidal lens models can represent the early-type galaxies that produce most lenses, although the correct dynamical normalization of the models is somewhat unclear (Keeton, Kochanek & Seljak 1997). What is perhaps less obvious is that they can also be used to represent spiral galaxies. An infinitely thin disk viewed in projection has an elliptical surface density, so with proper dynamical normalization ellipsoidal lens models can be used for spiral galaxy disks and halos (Keeton & Kochanek 1997b; Koopmans 1997).

3. General Features of Ellipsoidal Lens Models

The most obvious feature of ellipsoidal lens models is that they cannot fit 4-image lenses. Keeton et al. (1997) showed that singular isothermal models could not fit the 4-image lenses MG 0414+0534, PG 1115+080, H 1413+117, and B 1422+231. The fits do not improve significantly by adding a core radius or changing the radial profile (e.g. Keeton & Kochanek 1997a), which suggests that single-galaxy models cannot fit these lenses. The fits do improve dramatically, however, by adding a second source of shear to the ellipsoidal lens model (Keeton et al. 1997). Similarly, Witt & Mao (1997) found that a second shear is required to explain several 4-image lenses, including HST 12531−2914 and B 1608+656. Thus it appears that the need for two independent shears may be a generic feature of 4-image lenses.

The need for an additional shear is important for two reasons. First, the source of the shear must be explained. In PG 1115+080 and B 1422+231 (as well as the radio ring MG 0751+2716) the additional shear is known to come from the presence of a small group surrounding the primary lens galaxy (Hogg & Blandford 1994; Schechter et al. 1997; Kundić et al. 1997ab; Tonry 1997; Lehár et al. 1997). In other lenses the source of the shear is unknown. It could come from random perturbations along the line of sight, although these are not expected to be large enough to explain the required shears (Bar-Kana 1996; Keeton et al. 1997). Alternatively, it could be internal to the galaxy; for example, if the luminous and dark matter are triaxial with different triaxialities, the projected mass distributions can be misaligned and thus produce two shear axes (Keeton et al. 1997). Studying the additional shear can thus constrain galactic structure. If an external source can be identified then it can be separated from the galaxy to allow investigations of the galaxy itself; if no source can be identified, then the presence of the shear constrains the internal structure of the galaxy.

Second, the additional shear introduces new degeneracies into lens models. If the shear is treated as a simple external shear then there is a characteristic degeneracy between the magnitude of the shear and the ellipticity of the galaxy (see Figure 1). If the shear is treated as coming from a physical source, there can be degeneracies in the physical parameters of the source. For example, in

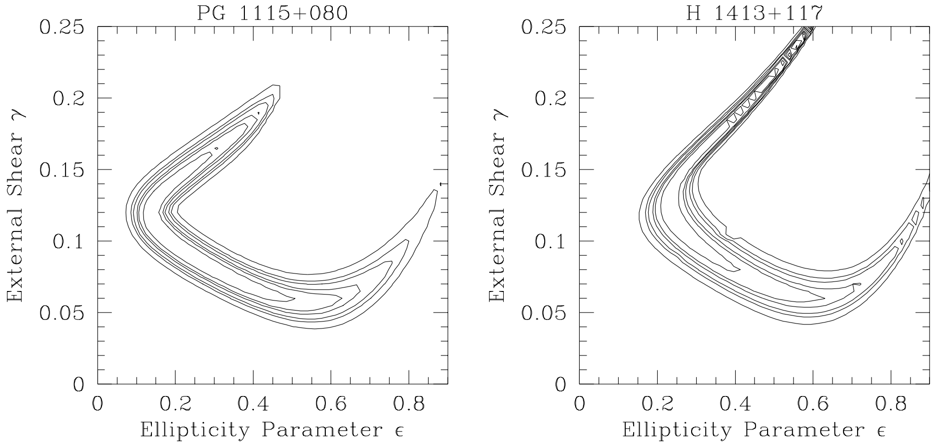

Figure 1. Results for singular isothermal ellipsoid plus external shear models. The contours are drawn at $\Delta\chi^2 = 2.30$, 4.61, 6.17, 9.21, 11.8, and 18.4, the 1σ, 90%, 2σ, 99%, 3σ, and 99.99% confidence levels for two parameters. Both lenses have good fits with $\chi^2/N_{dof} < 1$.

PG 1115+080 there is a degeneracy between the position and mass of the perturbing group (Keeton & Kochanek 1997a), although independent observations of the group velocity dispersion may help break this degeneracy (Kundić 1997a; Tonry 1997).

This "shear degeneracy" exists in addition to the familiar degeneracy in the radial profile, namely that point-image lenses with images spanning a narrow range of radii can say little about the radial structure of the mass distribution (e.g. Kochanek 1991; Wambsganss & Paczyński 1994). Both degeneracies make it difficult to identify a unique lens model, and hence to determine a unique estimate for H_0. Estimating H_0 thus requires surveying the parameter space to understand the systematic uncertainties in the lens model and their effects on H_0. Such surveys benefit strongly from using an ellipsoidal lens model with an additional shear, because the second shear axis introduces significant freedom in the models. For example, for PG 1115+080, Schechter et al. (1997) used an SIS galaxy with an independent SIS group to estimate $H_0 = 42$ km s^{-1} Mpc^{-1} but with no error bars. Keeton & Kochanek (1997a) allowed the galaxy to be an ellipsoid and found $H_0 = 51^{+14}_{-13}$ km s^{-1} Mpc^{-1}. In this case, using a two-shear model both produced an estimate less at odds with popular values for H_0, and allowed an estimate of the error bars due to systematic uncertainties.

The two degeneracies need not prevent good estimates of H_0 from lensing, because with improvements in the data the degeneracies can be reduced. Lens image positions can often be measured to ~ 5 mas accuracy, so there is not much room for improvement here; besides, in PG 1115+080 the image positions are already over-fit (Keeton & Kochanek 1997a), so improving the constraints would require improving the measurement accuracy by an order of magnitude. Pinning down the flux ratios, by contrast, would be quite useful. In radio lenses one can use radio flux ratios, which are less susceptible to microlensing than optical fluxes ratios. Alternatively, with light curves and time delay estimates one could try

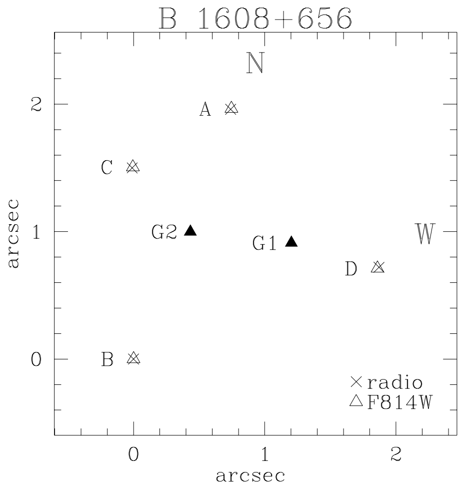

Figure 2. Schematic diagram of B 1608+656. A, B, C, and D are the four images of the background source, with crosses denoting the radio positions from Myers et al. (1995) and triangles denoting the HST positions. The filled triangles denote the positions of the two components of the lens galaxy (G1 and G2) as seen in F814W; relative to image B, the galaxy positions are G1= $(1.''20, 0.''91)$ and G2= $(0.''43, 1.''00)$. Lens models predict the time ordering of the images to be D–C–A–B.

to estimate intrinsic flux ratios. Another place to get good constraints is the lens galaxy. For PG 1115+080, Courbin et al. (1997) showed that reducing the galaxy position error bars from 50 mas to 15 mas reduced the model degeneracies and decreased the error bars in H_0 by a factor of 2. With good photometry it might be possible to use stellar dynamical arguments to constrain the profile of the mass model (e.g. Keeton & Kochanek 1997a). A final place for constraints that have not yet been fully exploited is the time delays. In 4-image lenses one can measure as many as three time delays. The mean delay determines H_0, but this leaves two time delay ratios that can be used to constrain lens models. Preliminary results suggest that the time delay ratio may provide the best constraint on the profile of the mass model (Keeton & Kochanek 1997a).

4. New Models of B 1608+656

B 1608+656, discovered in the Cosmic Lens All-Sky Survey (CLASS) lens survey, consists of four point-like radio images with $\sim 2''$ separations surrounding a $z = 0.630$ galaxy (Myers et al. 1995). Spectroscopic observations revealed that the source is not a quasar but rather a $z = 1.394$ poststarburst galaxy (Fassnacht et al. 1996), and HST observations confirmed that the optical images are extended (see Jackson, Nair & Browne 1997). The HST images also revealed the lens galaxy, which appears as an elongated galaxy ($\equiv$G1) with a circular blob ($\equiv$G2) off one end. G1 is prominent in both F814W (I) and F555W (V), while G2 is prominent in F814W but only barely visible in F555W. A schematic diagram of B 1608+656 is shown in Figure 2.

	SIE			SIS+shear		
	χ^2	ε	t_{DB} (h^{-1} days)	χ^2	γ	t_{DB} (h^{-1} days)
G1 unconstrained	765.6	0.38	34.1	795.2	0.06	15.9
G1 constrained	790.5	0.39	35.5	837.2	0.06	16.7

Table 1. Results for singular isothermal ellipsoid (SIE) and singular isothermal sphere plus external shear (SIS+shear) lens models. With G1 unconstrained $N_{dof} = 4$, and with G1 constrained $N_{dof} = 6$. All four models have an position angle between $68\overset{\circ}{.}5$ and $68\overset{\circ}{.}9$. The SIS+shear models have a critical radius of $b = 1\overset{''}{.}10$.

We can now use the ellipsoidal lens models to try to fit B 1608+656 and then use eq. (2) to predict time delays. For constraints we use the HST F814W image positions with 5 mas error bars, and the radio flux ratios with 20% error bars to account for any unknown time variation. Because the radio flux ratios are probably not susceptible to microlensing, the 20% error bars are very generous and mean that flux constraints are much weaker than the position constraints. For the galaxy, the appropriate constraints are less clear. If G1 and G2 are separate galaxies then it is appropriate to use their positions as constraints. If, however, they represent a single galaxy cut by a dust lane, then the appropriate galaxy position is somewhere between G1 and G2. Given this ambiguity, we considered models with no constraint on the galaxy position, as well as models with the galaxy position set to G1 with 50 mas error bars.

We note that from eq. (2) the time scale for the time delays is set by the factor $t_0 \equiv (D_l D_s/D_{ls})(1+z_l)/c$. We use an $\Omega_0 = 1$ cosmology for which $t_0 = 93.97\,h^{-1}$ days/arcsec^2. In an open cosmology or a λ-cosmology, t_0 can be larger by 10–15%.

4.1. Single-shear models

First we considered the simple lens models with a single source of shear. Table 1 summarizes the results for standard lens models with a singular isothermal galaxy, where the shear is generated either by adding an external shear or by using an ellipsoidal galaxy. The fits are terrible, with $\chi^2/N_{dof} > 130$ regardless of whether or not we constrain the galaxy. We could note that for all models the galaxy wants to sit not on G1 but rather $\sim 0\overset{''}{.}25$ closer to G2, but given the horrible fits this result is not very significant. One useful result from the models is that the time ordering of the images should be D–C–A–B, so the best-resolved time delays should be $\Delta\tau_{DB}$, or $\Delta\tau_{CB}$ if D is too faint. We quote the predicted value for $\Delta\tau_{DB}$. It is interesting that the shear models predict time delays about half as long as the ellipsoid models, but again given the terrible fits it is not reasonable to use these models to predict time delays.

We tried varying the profile of the galaxy by softening the isothermal model and changing to a modified Hubble model to approximate a constant mass-to-light ratio model. Figure 3 shows that the fits are still awful. Adding a core radius to the isothermal model only increases the χ^2. The more concentrated

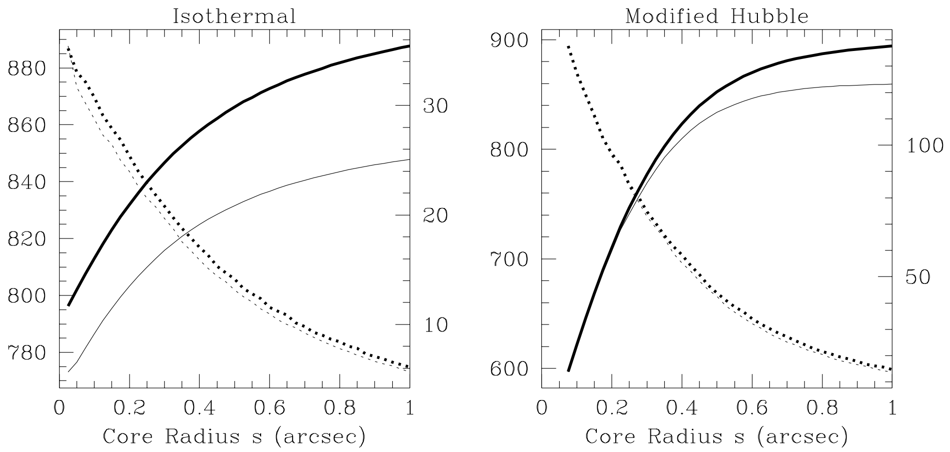

Figure 3. Results for single-galaxy lens models using an isothermal and a modified Hubble galaxy. Solid lines are χ^2 using the axis scale on the left, while dotted lines are the time delay t_{DB} in units of h^{-1} days using the axis scale on the right. Light lines show results with G1 unconstrained, while heavy lines show results with G1 constrained.

Hubble model can do only slightly better. It is possible that some intermediate concentration could do better still, but these results suggest that a single galaxy will have great difficulty explaining B 1608+656.

An obvious question is whether we have inflated the χ^2 by underestimating the error bars. The 20% flux error bars are large, and the fits are terrible even with the galaxy unconstrained, so the only possible source of trouble is the 5 mas position error bars. The HST image positions in F814W and F555W agree to ~ 3 mas and are consistent with the radio positions (which were given in Myers et al. 1995 to $0\farcs01$ without error bars). Thus it seems extremely unlikely that the error bars could change by an order of magnitude, which would be needed to make the single-galaxy models give a good fit.

4.2. Two-shear models

Thus B 1608+656 follows the trend of 4-image lenses that cannot be fit by single-shear models, so we examined a variety of two-shear models. The results for χ^2 and $\Delta\tau_{DB}$ are summarized in Figure 4. First, panel (a) shows the generic SIE plus external shear model used in Keeton et al. (1997). The model can give a good fit, giving $\chi^2/N_{dof} \sim 0.5\,(1.8)$ with the galaxy unconstrained (constrained). However, the best fit requires a weird model with both a very flattened galaxy ($\varepsilon \sim 0.9$ or $b/a \sim 0.2$) and a strong shear ($\gamma \sim 0.2$). This is much larger than shears expected from perturbations along the line of sight (Bar-Kana 1996; Keeton et al. 1997), so we must try to explain its source.

The obvious candidate for the shear is G2. Figure 4b–d show models treating G1 as an SIE free to move by constrained by the observed position, and G2 as an SIS or SIE. In Figure 4b G2 is an SIS fixed at the observed position, but with a variable size (critical radius b_{G2}) and redshift. The redshift z_{G2} is expressed in the parameter β such that

$$|\beta| = (D_{ij}D_s)/(D_jD_{is}) \tag{8}$$

$$\mathrm{sign}(\beta) = \begin{cases} +1 & z_{G2} > z_l \\ -1 & z_{G2} < z_l \end{cases} \tag{9}$$

(see Schneider et al. 1992, chapter 9), and $|\beta| \simeq 0.2$ (0.5) for $|z_{G2} - z_{G1}| \simeq 0.08$ (0.24). Making G2 larger does improve the fit, but not dramatically – it is still $\chi^2 \sim 600$ for $N_{dof} = 4$. G2 wants to sit at the same redshift as G1, consistent with the prediction from the correlation function that objects $0\farcs8$ apart are at the same redshift. Figure 4c shows that letting the position of G2 deviate from the observed position does not help either. Finally, Figure 4d shows that letting G2 be elliptical *does* dramatically improve the fit; this model with a rather large $b_{G2} = 0\farcs4$ can produce $\chi^2 = 15.7$ for $N_{dof} = 4$. However, again the good fit requires a rather strange model, where G1 is moderately flattened with $\varepsilon_{G1} = 0.32$ ($b/a = 0.72$) while G2 is much flatter with $\varepsilon_{G2} = 0.66$ ($b/a = 0.46$). This seems to be opposite to the observed luminous distributions, where G1 is large and flattened and G2 is smaller and round.

These results suggest that B 1608+656 requires a non-trivial lens model. The data cannot be fit by a single ellipsoidal galaxy, and not even by an ellipsoidal galaxy supplemented by a spherical G2. A spherical mass distribution representing a nearby group is insufficient to generate the tidal shear in PG 1115+080 (Schechter et al. 1997; Keeton & Kochanek 1997), but in B 1608+656 it seems that G2 is close enough that a spherical model is sufficient. It may be possible to find a reasonable model by combining the preliminary approaches taken here – representing G2 with an ellipsoidal mass distribution, letting its position deviate slightly from the observed position, and using a reasonable critical radius b_{G2}. Alternatively, if two-shear models do not fit then perhaps we must invoke three-shear models. In any case, it will be crucial to explore the entire parameter space to identify any degeneracies.

5. Conclusions

There is mounting evidence that ellipsoidal mass distributions cannot explain many or even most of the 4-image lenses in quantitative detail. Generically, it seems that some additional independent shear is required. The additional shear introduces a new degeneracy into lens models which has implications for both astrophysics and cosmology. First, identifying an external source for the shear can tell us about the properties of galaxies, for example that they often have perturbers consisting of small groups near or containing the primary lens galaxy as expected from the correlation function (Keeton et al. 1997). Alternatively, failing to identify a source for the shear constrains the internal structure of galaxies. Second, the model degeneracies mean that it is difficult to identify a unique lens model for estimating H_0. Determining H_0 from lensing requires surveys of lens models to understand systematic uncertainties in the models and their effects on H_0.

Acknowledgments. We are grateful to E. Falco for analyzing the archive HST images of B 1608+656. CRK is supported by ONR-NDSEG grant N00014-

93-I-0774. CSK is supported by NSF grant AST-9401722 and NASA ATP grant NAG5-4062.

References

Bar-Kana, R. 1996, ApJ, 468, 17

Courbin, F., Magain, P., Keeton, C. R., Kochanek, C. S., Vanderriest, C., Jaunsen, A. O., & Hjorth, J. 1997, A&A, in press (also preprint astro-ph/9705093)

Hogg, D. W., & Blandford, R. D. 1994, MNRAS, 268, 889

Jackson, N., Nair, S., & Browne, I. W. A. 1997, in Observational Cosmology with the new radio surveys, ed. M. Bremer, N. Jackson & I. Perez-Fournon (Dordrecht: Kluwer), also `http://www.jb.man.ac.uk/~njj/glens/ceres.html`

Kassiola, A., & Kovner, I. 1993, ApJ, 417, 459

Keeton, C. R., Kochanek, C. S., & Seljak, U. 1997, ApJ, 482, 604

Keeton, C. R., & Kochanek, C. S. 1997a, ApJ in press (also preprint astro-ph/9611216)

Keeton, C. R., & Kochanek, C. S. 1997b, ApJ submitted (also preprint astro-ph/9705194)

Kochanek, C. S. 1991, ApJ, 373, 354

Koopmans, L. V. E. 1997, in preparation

Kormann, R., Schneider, P., & Bartelmann, M. 1994, A&A, 284, 285

Kundić, T., Cohen, J. G., Blandford, R. D., & Lubin, L. M. 1997a, preprint astro-ph/9704109

Kundić, T., Hogg, D. W., Blandford, R. D., Cohen, J. G., Lubin, L. M., & Larkin, J. E. 1997b, preprint astro-ph/9706169

Lehár, J., Burke, B. F., Conner, S. R., Falco, E. E., Fletcher, A. B., Irwin, M., McMahon, R. G., Muxlow, T. W. B., & Schechter, P. L. 1997, preprint astro-ph/9702191

Schechter, P.L. et al. 1997, ApJ, 475, L85

Schneider, P., Ehlers, J., & Falco, E. E. 1992, Gravitational Lensing (New York: Springer)

Tonry, J. L. 1997, preprint astro-ph/9706199

Wambsganss, J., & Paczyński, B. 1994, AJ, 108, 1156

Witt, H. J., & Mao, S. 1997, preprint astro-ph/9702021

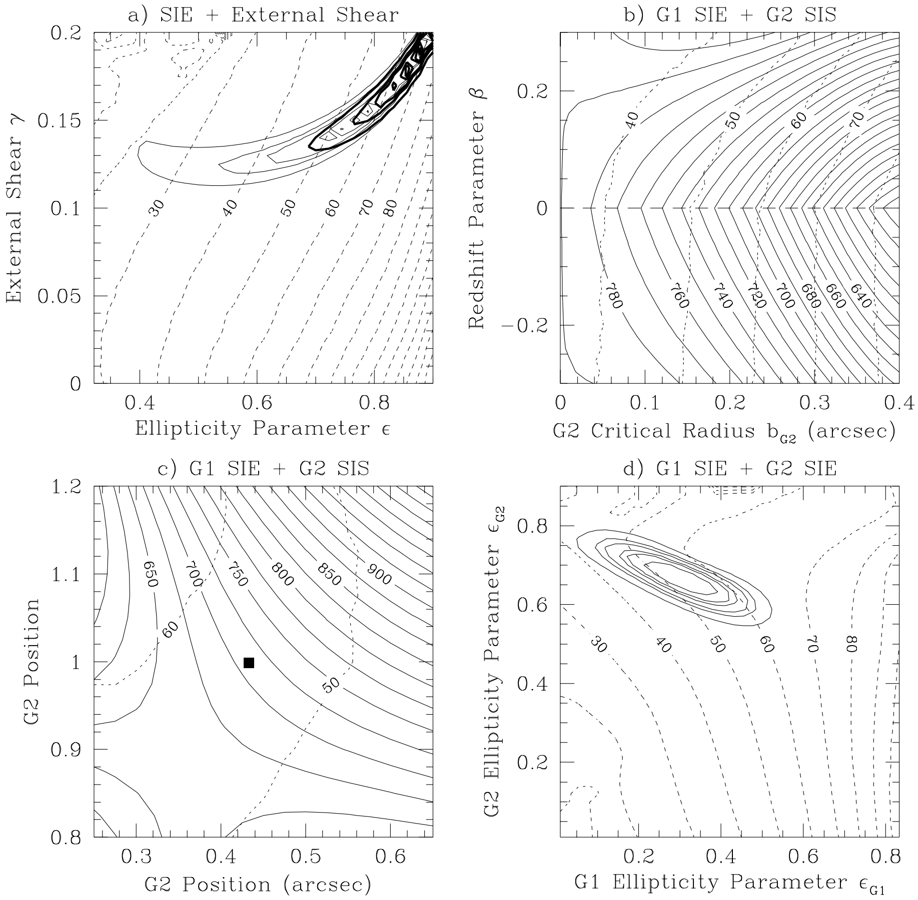

Figure 4. Results for various classes of two-shear models. (a) Singular isothermal ellipsoid (SIE) plus external shear models. (b) Models treating G1 as an SIE, and G2 as an SIS fixed at the F814W position. (c) Models treating G2 as an SIS with $b_{G2} = 0\farcs2$, varying the position of G2. (d) Models treating G2 as an SIE with $b_{G2} = 0\farcs4$, fixed at the F814W position. In (a) and (d) the contours are drawn at $\Delta\chi^2 = 2.30$, 4.61, 6.17, 9.21, 11.8, and 18.4, the 1σ, 90%, 2σ, 99%, 3σ, and 99.99% confidence levels for two parameters. In (a) the light (heavy) contours show the χ^2 with the galaxy unconstrained (constrained), where the best-fit models have $\chi^2 = 0.9$ (7.4) for $N_{dof} = 2$ (4). In (d) the best-fit model has $\chi^2 = 15.7$ for $N_{dof} = 4$. In (b) and (c) the χ^2 contours are as labeled. In all panels the dotted contours are contours of $\Delta\tau_{DB}$ in units of h^{-1} days.